Supporting Information for

Mechanical Vibrations of Atomically Defined Metal Clusters: From Nano- to Molecular-Size Oscillators

Paolo Maioli,[1*] Tatjana Stoll,[1,2] Huziel E. Sauceda,[3] Israel Valencia,[4] Aude Demessence,[5] Franck Bertorelle,[1] Aurélien Crut,[1] Fabrice Vallée,[1] Ignacio L. Garzón,[6] Giulio Cerullo,[2] and Natalia Del Fatti[1]

[1]Institut Lumière Matière, Université de Lyon, CNRS, Université Claude Bernard Lyon 1, F-69622 Villeurbanne, France

[2]Dipartimento di Fisica, Politecnico di Milano, IFN-CNR, Piazza L. da Vinci 32, I-20133 Milano, Italy

[3]Fritz-Haber-Institute der Max-Planck-Gesellschaft, 14195 Berlin, Germany

[4]Facultad de Estudios Superiores-Iztacala, Universidad Nacional Autónoma de México, 54090 Tlanepantla, Estado de México, México

[5]Institut de Recherches sur la Catalyse et l'Environnement de Lyon (IRCELYON), Université de Lyon, CNRS, Université Claude Bernard Lyon 1, F-69622 Villeurbanne, France

[6]Instituto de Física, Universidad Nacional Autónoma de México, Apartado Postal 20-364, 01000 CDMX, México

*paolo.maioli@univ-lyon1.fr

Table of Contents of the Supporting Information

I. Ligand-protected cluster synthesis

Sample *a*, containing $Au_{10}(SPhtBu)_{10}$ clusters in toluene, was synthesized following a reaction reported in ref 1. The characterization of the sample by X-ray powder diffraction (XRD), electrospray ionization mass spectroscopy (ESI-MS) and UV-visible spectroscopy shows its purity (Figure S1 in the Supporting Information). Its structural morphology, deduced theoretically and later confirmed by measurements of optical spectra and XRD profiles,[1–3] is characterized by two interconnected Au_5 rings, the equal Au-to-ligand ratio preventing the formation of a metal core with delocalized electrons, which results in the absence of metallic properties. Sample *b*, consisting of $Au_{15}(SG)_{13}$ clusters in water, was obtained following the synthesis published in ref 4, and dissolved in water before use. Two different structures were theoretically proposed by different authors.[5,6] Sample *c*, consisting of $Au_{25}(SCH_2CH_2Ph)_{18}$ clusters in DMF, is one of the most studied compositions.[7] It was obtained here following synthesis process reported in ref 8 and its characterization by XRD, ESI-MS and UV-visible spectroscopy points out its purity (Figure S2). Its structure is composed by an inner core with a 13-atom icosahedron and 12 Au atoms bridged by the thiolate ligands in the outer shell.[8,9] $Au_{25}(SG)_{18}$ clusters (sample *d*) in gel were obtained following the synthesis reported in ref 10 and polyacrylamide gel electrophoresis (separating gel: acrylamide 30% (acrylamide/bis-(acrylamide) 94:6) and eluting buffer: 192 mM glycine and 25 mM tris(hydroxymethylamine)). $Au_{102}(SPhCOOH)_{44}$ clusters dispersed in water (sample *e*) were obtained by following the synthesis reported in ref 11, their characterizations confirming their purity (Figure S3). This was the first cluster composition whose crystal structure was established[12] and is formed by a metallic Au_{79} core (Au_{39} inner core and Au_{40} outer shell) protected by a $Au_{23}(SR)_{44}$ layer.[12,13] Sample *f*, which consists of size-dispersed Au nanoparticles in DMF with mean diameter of (3.5 ± 0.7) nm (number of Au atoms around 1350) and functionalized with SCH_2CH_2Ph ligands, is synthesized and characterized by XRD, transmission electron microscopy (TEM) and UV-

visible absorption (Figure S4). The acoustic response of these large nanospheres is used as a reference for discussing the transition in the acoustic response from nanoparticles to smaller clusters.

II. Ligand-protected cluster characterization

This section provides detailed information on the structural and optical characterization of investigated ligand-protected atomically-defined clusters Au_n (n = 10, 25, 102) and larger (D = 3.5 nm) Au nanoparticles.

Chemicals

All chemicals: 2-Phenylethanethiol, 4-mercaptobenzoic acid, 4-tert-butylbenzenethiol, tetrachloroauric acid hydrate (HAuCl4.xH2O, 52% Au basis), tetraoctylammonium bromide, ammonium actetate, sodium borohydride, sodium hydroxide, toluene, dichloromethane (CH_2Cl_2), methanol (MeOH) and N,N-dimethylformamide (DMF) were purchased from Aldrich Chemical Company, Inc. All reagents and solvents were of commercial quality and used without further purification. The glassware used in the syntheses was cleaned with aqua regia and then rinsed with copious amount of distilled water, then dried overnight prior to use. All reactions were carried out in atmospheric conditions.

Tools

X-ray power diffraction (XRD) was carried out on a Bruker D8 Advance A25 diffractometer using Cu Kα radiation equipped with a 1-dimensional position-sensitive detector (Bruker LynxEye). Small angle X-ray scattering was recorded between 0.45° and 7° (2θ) with 0.01° steps and 2 s per step (25 min for the scan). Automatic variable divergence slit was set to 20 mm and the detector aperture to 59 channels (0.9°). Wide angle X-ray scattering was recorded

between 4° and 90° (2θ) with 0.02° steps and 0.5 s per step (28 min for the scan). Divergence slit was fixed to 0.2° and the detector aperture to 189 channels (2.9°).

The mass spectra (ESI-MS) were recorded on a hybrid quadrupole time-of-flight mass spectrometer (MicroTOFQ-II, Bruker Daltonics, Bremen) with an Electrospray Ionization ion source. The gas flow of spray gas is 0.6 bar and the capillary voltage is 4.5 kV. Mild conditions were used for the ions transfer to keep intact the functionalized nanoclusters. The solutions are infused at 180 μL/h in a mixture of solvents (methanol/dichloromethane/water 45/40/15). The calibration was done with cesium iodide and tune mix (Agilent).

The UV-visible spectra of solutions were carried out on an Agilent 8453 diode-array spectrophotometer. Spectrophotometer interval is 1.0 nm and integration time is 0.5 s.

Transmission electron microscopy (TEM) is carried out on a JEOL 2010 LaB6 microscope operating at 200 kV. To observe individual particles, sample is first dispersed in N,N-dimethylformamide (average 0.3 mg per mL), then one drop of this colloidal solution is dispersed in around 5 mL of ethanol and quickly filed on a carbon-coated copper grid. Solvent is then let evaporate at ambient temperature for at least one hour before TEM analysis.

Cluster characterization

Purity of $Au_{10}(SPhtBu)_{10}$ clusters (sample *a*) was confirmed by XRD, ESI-MS and UV-visible absorption (Figure S1). Purity of $Au_{25}(SCH_2CH_2Ph)_{18}$ clusters (sample *c*) was confirmed by XRD, ESI-MS and UV-visible adsorption (Figure S2). Analogously, purity of $Au_{102}(SPhCOOH)_{44}$ clusters (sample *e*) is confirmed by XRD, ESI-MS and UV-visible absorption signals reported in Figure S3. 3.5 nm Au nanoparticles (sample *f*) are characterized by XRD, TEM imaging and UV-visible absorption (Figure S4).

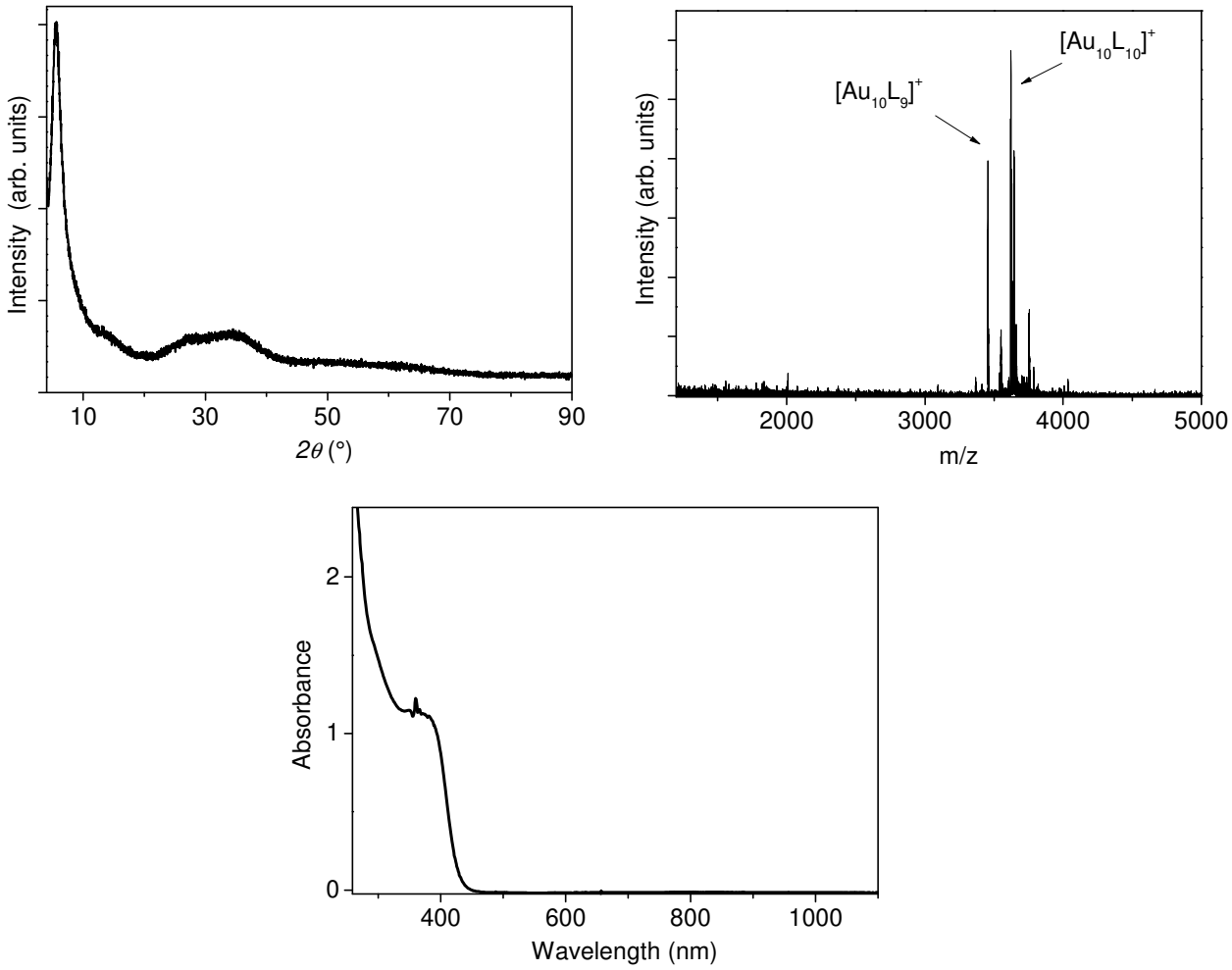

Figure S1. Characterization of $Au_{10}(SPhtBu)_{10}$ clusters (sample *a*). (left) XRD pattern. The peak at 5.57° corresponds to a distance of 1.6 nm between the centers of two particles. (right) ESI mass spectrum of $Au_{10}(SPhtBu)_{10}$ and its fragmentation. (bottom) UV-visible spectrum of $Au_{10}(SPhtBu)_{10}$ in CH_2Cl_2.

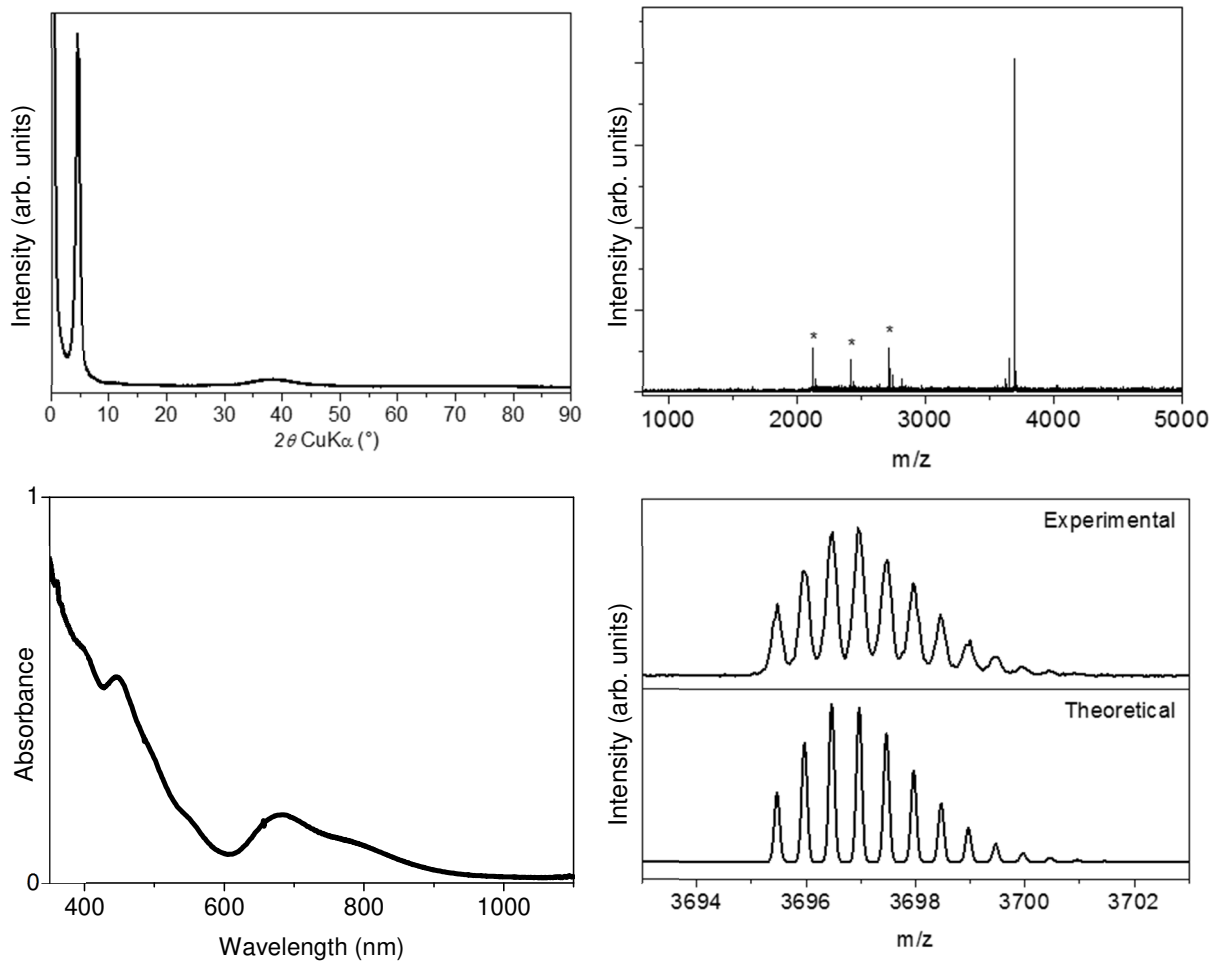

Figure S2. Characterization of $Au_{25}(SCH_2CH_2Ph)_{18}$ clusters (sample *c*). (top left) Experimental XRD patterns. The peak at 4.55° corresponds to a distance of 1.9 nm between the centers of two particles. (top right) Wide-range ESI mass spectrum (main peak at m/z = 3695.4623 Th). Peaks marked * correspond to the standard used to calibrate the spectra. (bottom right) The isotopic pattern of main peak (m/z theoretical = 3695.4638, error = -0.4 ppm), together with the simulated pattern and a resolving power of 15000. (bottom left) UV-visible spectrum of $Au_{25}(SCH_2CH_2Ph)_{18}$ in DMF.

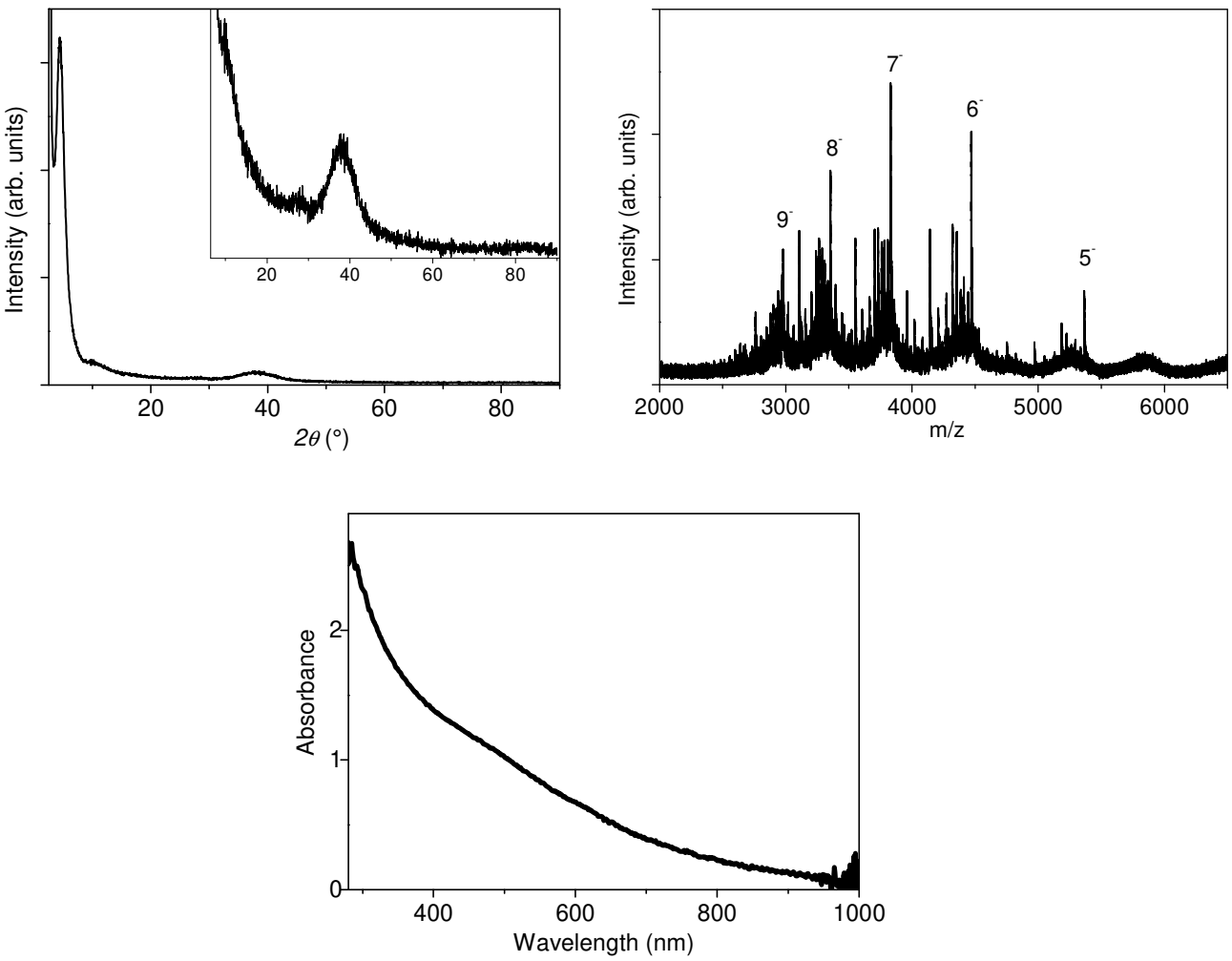

Figure S3. Characterization of $Au_{102}(SPhCOOH)_{44}$ (sample *e*). (left) XRD pattern. The peak at 4.45° corresponds to a distance of 2.0 nm between the centers of two particles. (right) ESI mass spectrum. The main peaks correspond to the fragmentation of $Au_{102}(SPhCOOH)_{44}-nH^+]^{n-}$. (bottom) UV-visible spectrum of $Au_{102}(SPhCOOH)_{44}$ in water.

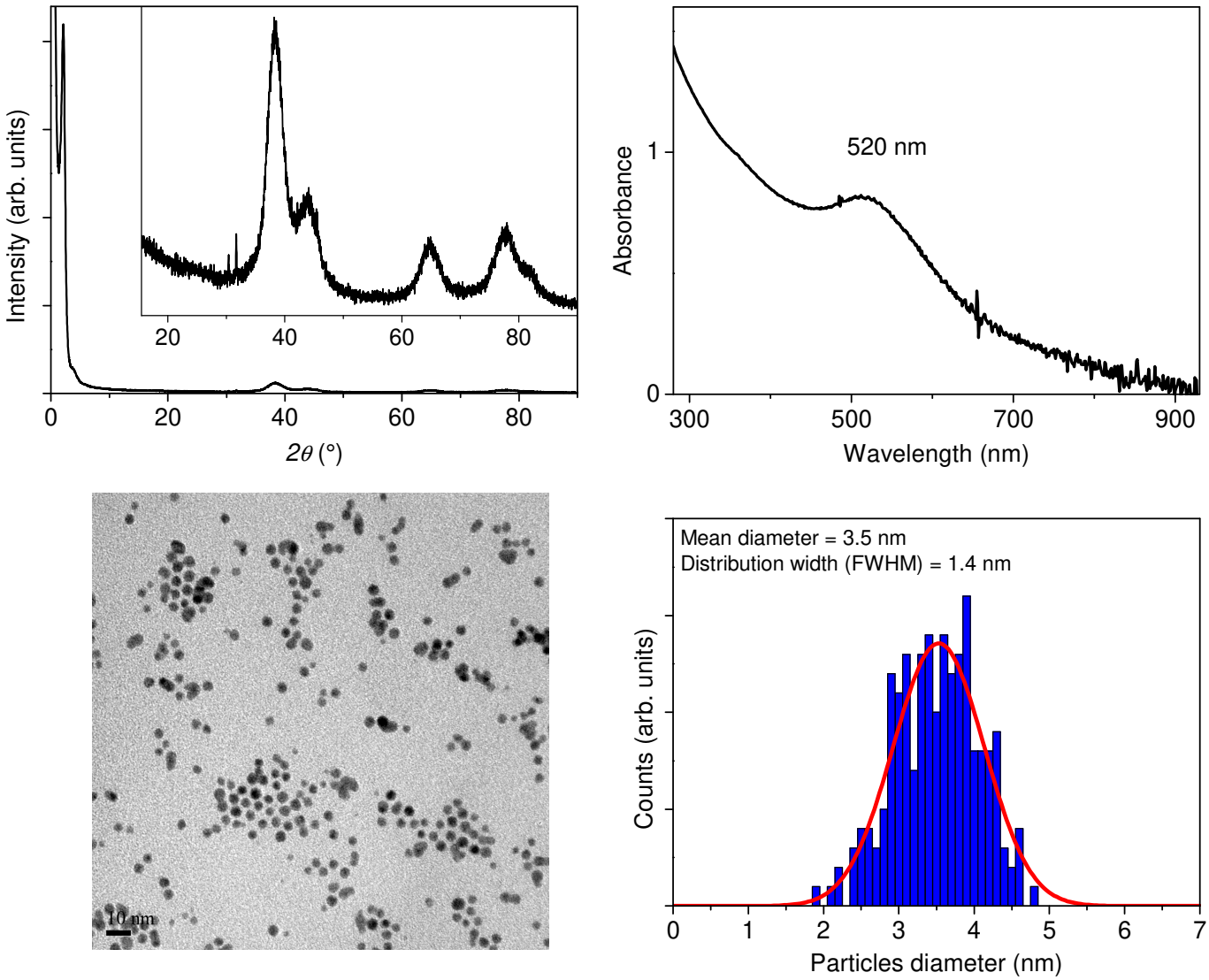

Figure S4. Characterization of 3.5 nm Au nanoparticles (sample f). (top left) XRD pattern. The peak at 2.11° corresponds to a distance of 4.2 nm between the centers of two particles. (top right) UV-visible spectrum of sample f in DMF, which indicates the presence of surface plasmon resonance at 520 nm. (bottom) TEM images of sample f and particle size distribution.

III. Time-resolved ultrafast transient absorption spectroscopy

The optical setup for ultrafast transient absorption spectroscopy on small clusters is based on a regeneratively amplified femtosecond Ti:Sapphire laser system, delivering 100-fs pulses at 800 nm wavelength and 1-kHz repetition rate. In a first configuration (setup 1), the system drives two non-collinear optical parametric amplifiers (NOPAs)[14] followed by chirped mirror compressors, each of which generates tunable sub-20-fs pulses in the visible range acting as pump and probe pulses. In a second configuration (setup 2), the output of a near-infrared NOPA is frequency-doubled in a β-barium borate (BBO) crystal to achieve longer (50-100 fs) blue pump pulses, while a fraction of the 800-nm beam is focused in either a sapphire or a CaF_2 plate to generate a broadband white light continuum used as a probe (the latter allowing a more blue-shifted spectrum than the former). Pump and probe pulses are superimposed on the sample (gel or cuvette for liquids) and the differential transmission (ΔT/T) spectrum of the probe is measured by an optical multichannel analyzer working single-shot at 1-kHz repetition rate.[15] Pump pulse energy at the sample ranges from E_{pump} = 20 to 200 nJ. Time-resolved ΔT/T signals recorded with these setups are shown in Figure 1 and in Figure S5. Experiments on larger nanoparticles (Figure S6) were also performed with a quasi-monochromatic probe using a Ti:sapphire regenerative amplifier (setup 3) delivering ~ 100 fs pulses at 800 nm with a repetition rate of 250 kHz, associated to a BBO crystal (for blue pump configuration, E_{pump} ~ 1 nJ) and to an optical parametric amplifier system (for visible probe). With this setup, high sensitivity detection of the pump-induced changes is achieved by mechanical chopping of the pump beam at 40 kHz and lock-in detection of the probe transmission change. Stability of all the samples under femtosecond laser irradiation was verified by systematically proving no change in their linear absorption spectra acquired before and after each time-resolved

acquisition. The frequencies extracted from transient optical signals do not depend on the setup and on the experimental parameters used (see for example Figures S5d and S6b).

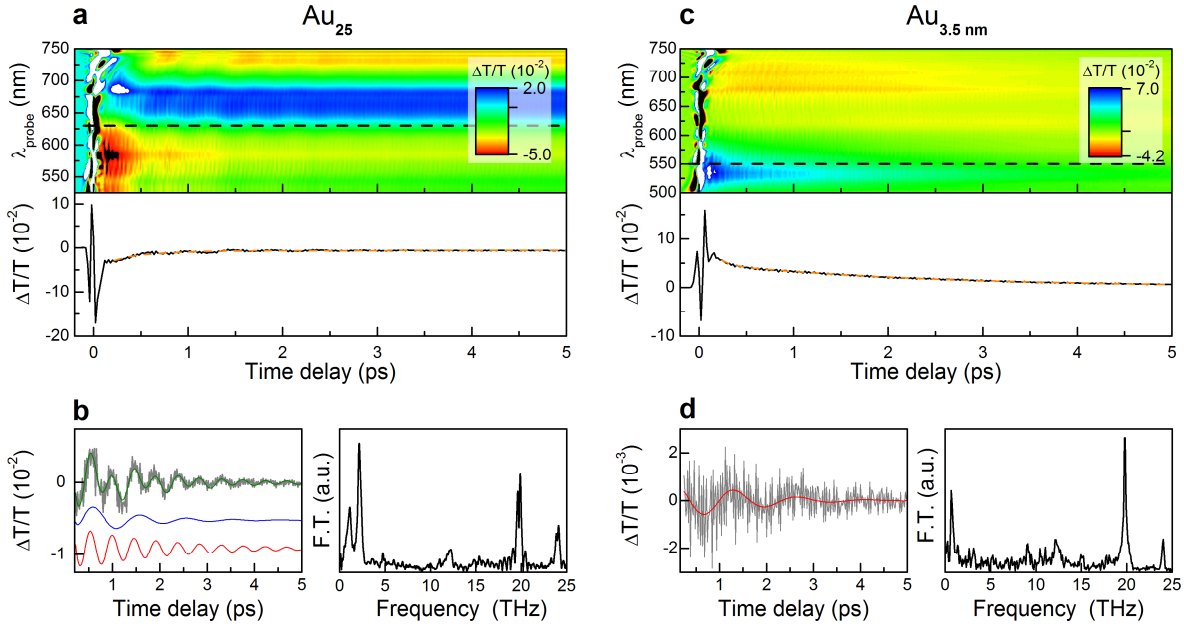

Figure S5. Ultrafast time-resolved transient absorption signals of sample c and sample f. (a) Upper panel: transient transmission change (ΔT/T) as a function of probe wavelength and pump-probe time delay, measured on sample *c* with setup 1, λ_{pump} = 590 nm. Lower panel: ΔT/T time trace (solid black line) at probe wavelength λ_{probe} = 630 nm (dashed line) and its fit with a slowly varying exponential function (dashed orange line). (b) Left: oscillating part of the signal (solid gray line), its fit with damped periodic functions (red and blue lines for shorter and longer periods, vertically shifted for clarity; green line as the sum of the two contributions). Right: Fourier transform of the oscillating contribution. The two lower frequency peaks correspond to QM and BM, while peaks at 20 and 25 THz correspond to resonances in the solvent (DMF). (c) Same as (a) measured on sample *f*, with setup 1, λ_{pump} = 590 nm and λ_{probe} = 550 nm. (d) Left: oscillating part of the signal (gray line) and its fit (red line) taking into account the effect of size distribution of sample *f*.[16] Right: Fourier transform of the oscillating contribution. Note that, due to the short pulse duration ($\lesssim$ 20 fs), strong oscillations corresponding to high-frequency solvent resonances are clearly visible in the time-domain signal (gray line in (d)).

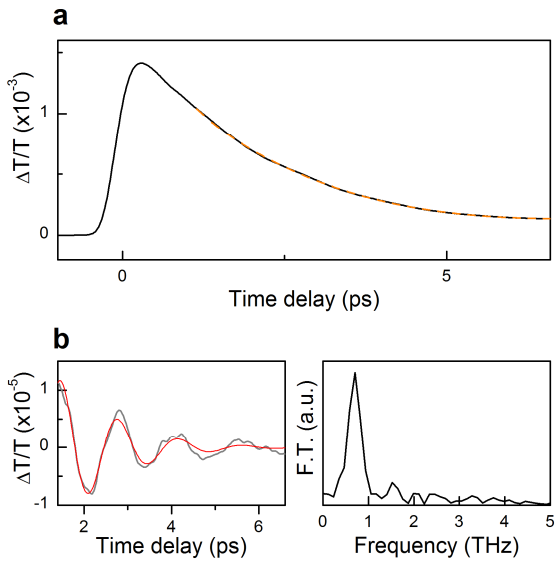

Figure S6. Ultrafast time-resolved transient absorption signal measured with the higher repetition-rate quasi-monochromatic laser setup (setup 3). (a) Transient transmission change (ΔT/T) on sample *f* (solid black line), measured with λ_{pump} = 400 nm and λ_{probe} = 545 nm and its fit with a slowly varying exponential function (dashed orange line). (b) Left: oscillating part of the signal (gray line) and its fit (red line) taking into account the effect of size distribution.[16] Note that the same BM frequency is extracted using either this setup or setup 1 (Figure S5d).

IV. DFT computations of vibrational frequencies

Density functional theory within the generalized gradient approximation using the Perdew-Becke-Ernzerhof[17] parametrization for the exchange correlation functional (DFT-GGA-PBE), as implemented in the Gaussian09 code,[18] was used for the cluster force and energy calculations. The inner core shells of the gold atoms were approximated by a scalar relativistic pseudopotential, while the outermost valence electrons were described through the LANL2DZ basis set.[19] An all-electron description was utilized with the basis sets 6-31G(d,p) for the S, and the 3-21G for the C and H atoms.[20,21] Given the much larger number of valence electrons involved in the bigger clusters studied, for $Au_{68}(SR)_{34}$, $Au_{102}(SR)_{44}$, and Au_{79}, (chosen as the inner core of $Au_{102}(SR)_{44}$) smaller basis sets were considered: LANL2MB for the Au atoms,[19] and STO-3G for the H ones.[22] Structural optimizations were performed using a tight convergence criterion, with a force tolerance of $5x10^{-4}$ eV/Å. For a further increment in the feasibility of the DFT calculations, the C-H bonds were frozen in the structural optimization of the $Au_{68}(SR)_{34}$ and $Au_{102}(SR)_{44}$ clusters. The level of theory mentioned above has been used before for calculations of structural and vibrational properties of ligand-protected gold clusters, providing reliable trends that agree with experimental information.[23–25]

Figures 3 and S7 show morphologies and DFT-computed vibrations of ligand-protected clusters, while the ones for bare clusters are summarized in Figure S8 (see also animation movies in the Supporting Information). The initial structures used in the relaxation of the ligand-protected Au clusters were obtained from various sources. For the smallest cluster $[Au_{12}(SR)_9]^+$, the initial structure formed by an octahedral Au_6 core protected by 3 dimeric staple motifs was taken from previous theoretical works.[23,26] It should be noticed that this cluster is studied in its cationic state to satisfy the 2e- shell closing count required by the spherical superatom complex (SAC) model that explains the cluster stability.[27] There are two slightly

different structures proposed for the $Au_{15}(SR)_{13}$ cluster,[5,6] resulting in different mechanical vibration periods for the two considered structures (solid green left- and right-pointing triangles in Figure 2b). In both of them, there is a tetrahedral Au_4 core, but in one case (Au15(i), see Figure S7) is protected by two trimer staple motifs surrounded by a $Au_5(SR)_5$ ring,[5] whereas in the other (Au15(ii)) it is covered by one tetramer $Au_4(SR)_5$ and one heptamer $Au_7(SR)_8$ motifs.[6] These structures are close in energy and yield optical absorption spectra in qualitative agreement with the experiment. The structure of the $Au_{18}(SR)_{14}$ cluster is available after it was determined by two experimental groups using single-crystal X-ray crystallography (XRC). Both groups coincide in their results, indicating that this cluster is formed by a bi-octahedral Au_9 kernel protected by staple motifs including one tetramer, one dimer, and three monomers.[28,29] Note that the value of BM period previously computed for $Au_{18}(SR)_{14}$ in ref 24 (yellow dot in Figure 2b) is slightly larger due to the difference in the considered cluster morphology. Likewise, two experimental[8,30] and one theoretical[9] groups provided the structure of the anionic $[Au_{25}(SR)_{18}]^-$ cluster. It consists of a 13-atom icosahedral core protected with six dimeric staple motifs. This cluster is studied in the anionic state to be stabilized by the 8e- and satisfy the shell closing rule of the spherical SAC model.[27] Our calculations were done using the atomic coordinates from ref 30. XRC[31] and theoretical calculations[32] also provided the structure and atomic coordinates of the $Au_{38}(SR)_{24}$ cluster. It is formed by a 23-atom bi-icosahedral core protected by six dimeric and three monomeric staple motifs. DFT calculations predicted the structures and provided the atomic coordinates of the $Au_{44}(SR)_{28}$ cluster that consists of a 26-atom fcc core capped with eight dimeric and two monomeric staple motifs,[33] and of the $Au_{68}(SR)_{34}$ cluster, formed by a Au_{50} core with a Marks-decahedral Au_{18} inner core protected by 14 monomeric and two dimeric staple motifs.[34] The atomic coordinates of the $Au_{102}(SR)_{44}$ cluster were taken from the XRC data reported in ref 12.

The initial neutral structures for cluster relaxation were taken from refs 35 and 36, except for the Au_{79} cluster, which was taken from the relaxed structure of the $Au_{102}(SR)_{44}$ core used in this work.[37]

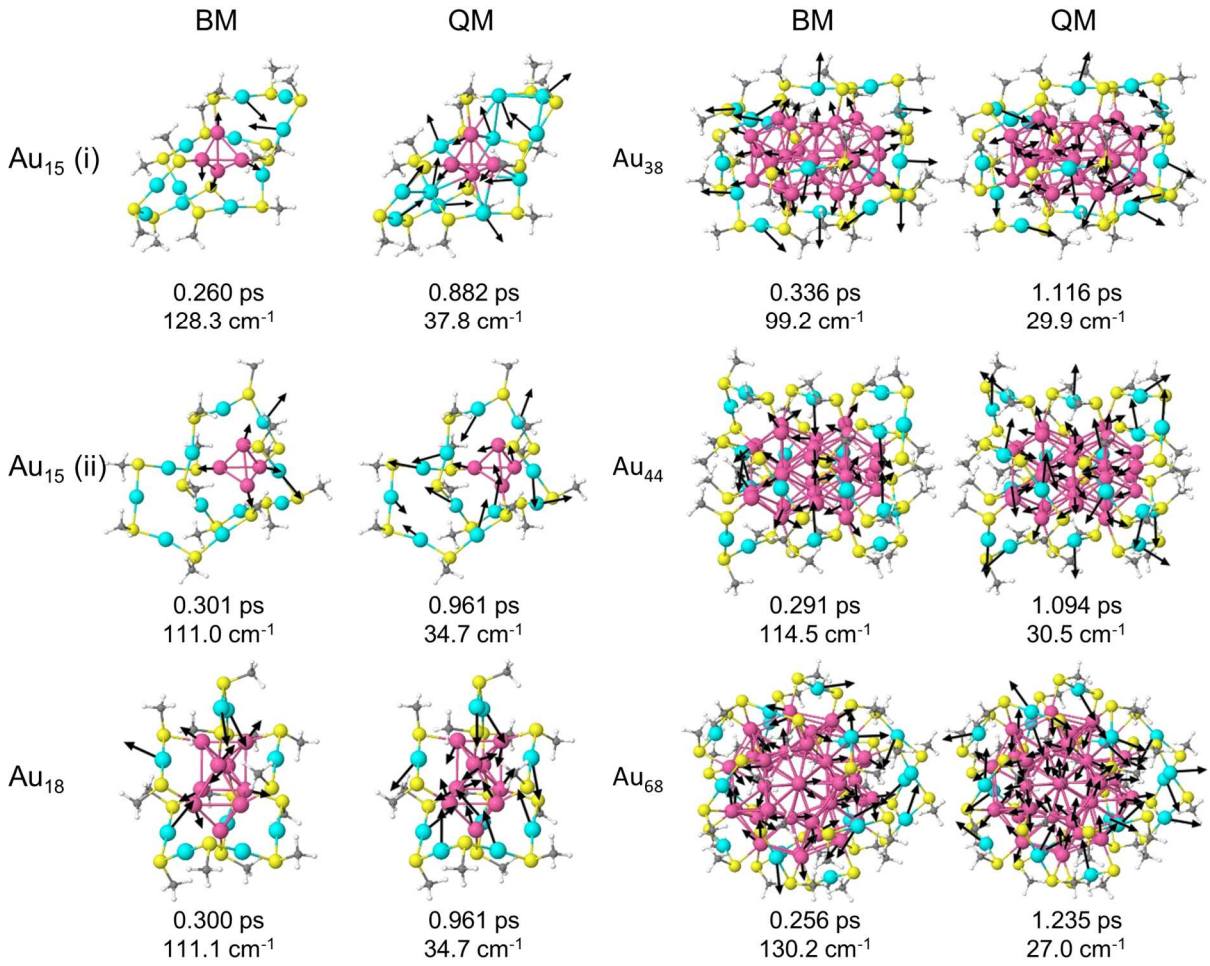

Figure S7. Clusters structures, displacement of selected atoms (arrows) and mechanical vibrations BM and QM periods deduced by DFT computations on $Au_{15}(SCH_3)_{13}$ ((i) and (ii) corresponding to structures theoretically determined in refs 5 and 6 respectively), $Au_{18}(SCH_3)_{14}$, $Au_{38}(SCH_3)_{24}$, $Au_{44}(SCH_3)_{28}$, $Au_{68}(SCH_3)_{34}$ for both breathing-like (BM) and quadrupolar-like (QM) modes. Color code: Au core atoms (magenta), Au external atoms (blue), S atoms (yellow), C atoms (gray) and H atoms (white). BM and QM displacements are also shown in the animation files included in the Supporting Information.

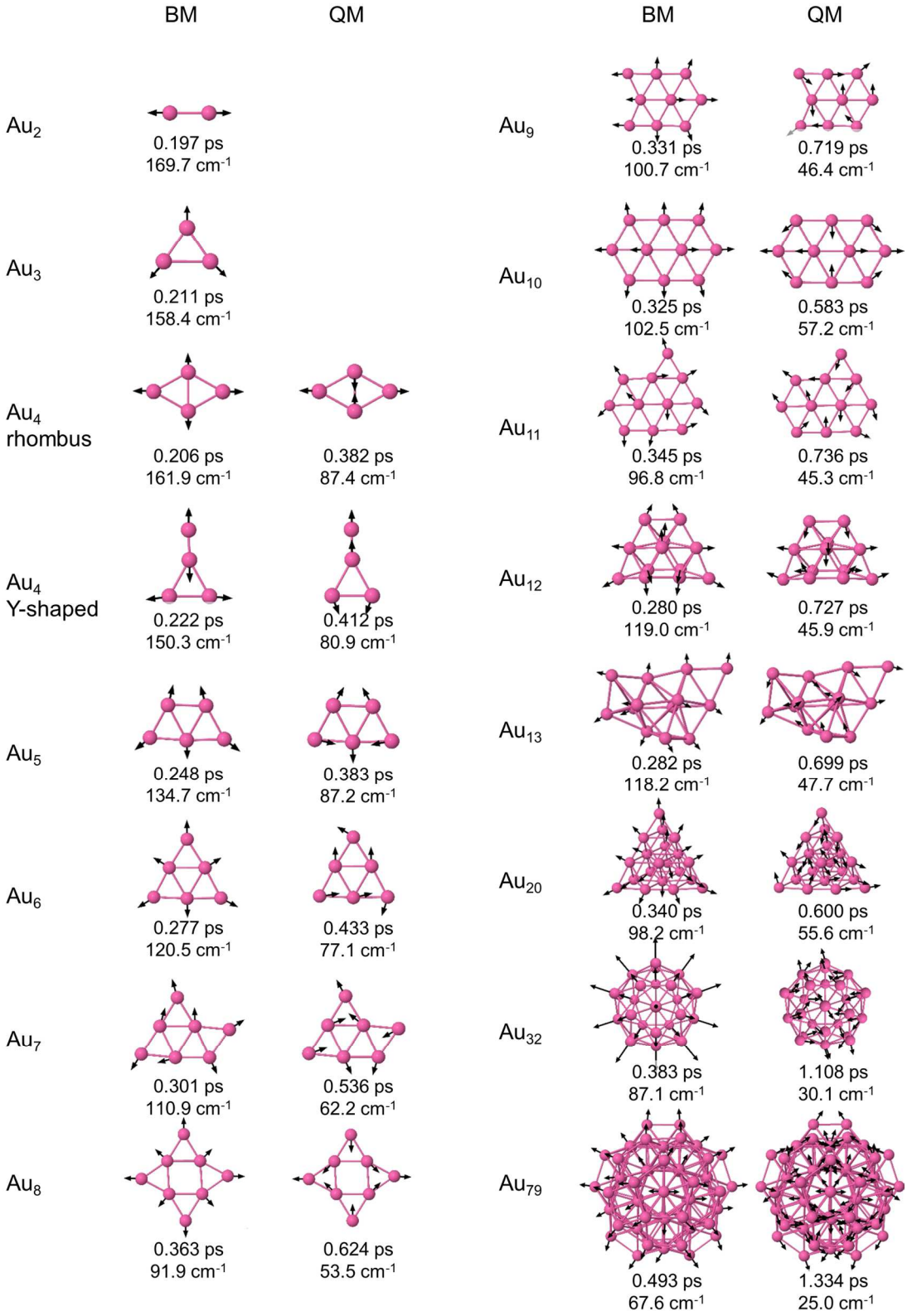

Figure S8. Computed atomic structures, BM and QM frequencies for Au_n bare clusters from *n* = 2 to 79. Arrows show atom displacement. BM and QM displacements are also shown in the animation movies included in the Supporting Information.

References

(1) Wiseman, M. R.; Marsh, P. A.; Bishop, P. T.; Brisdon, B. J.; Mahon, M. F. *J. Am. Chem. Soc.* **2000**, *122* (50), 12598–12599.

(2) Liu, Y.; Tian, Z.; Cheng, L. *RSC Adv.* **2016**, *6* (6), 4705–4712.

(3) Bertorelle, F.; Russier-Antoine, I.; Calin, N.; Comby-Zerbino, C.; Bensalah, A.; Guy, S.; Dugourd, P.; Brevet, P.-F.; Sanader, Z.; Krstic, M.; Bonacic-Koutecky, V.; Antoine, R. *J. Phys. Chem. Lett.* **2017**, *8*, 1979–1985.

(4) Russier-Antoine, I.; Bertorelle, F.; Vojkovic, M.; Rayane, D.; Salmon, E.; Jonin, C.; Dugourd, P.; Antoine, R.; Brevet, P.-F. *Nanoscale* **2014**, *6* (22), 13572–13578.

(5) Jiang, D.; Overbury, S. H.; Dai, S. *J. Am. Chem. Soc.* **2013**, *135* (24), 8786–8789.

(6) Tlahuice-Flores, A.; Jose-Yacamán, M.; Whetten, R. L. *Phys. Chem. Chem. Phys.* **2013**, *15* (45), 19557–19560.

(7) Jin, R.; Zeng, C.; Zhou, M.; Chen, Y. *Chem. Rev.* **2016**, *116* (18), 10346–10413.

(8) Zhu, M.; Aikens, C. M.; Hollander, F. J.; Schatz, G. C.; Jin, R. *J. Am. Chem. Soc.* **2008**, *130* (18), 5883–5885.

(9) Akola, J.; Walter, M.; Whetten, R. L.; Häkkinen, H.; Grönbeck, H. *J. Am. Chem. Soc.* **2008**, *130* (12), 3756–3757.

(10) Shibu, E. S.; Muhammed, M. A. H.; Tsukuda, T.; Pradeep, T. *J. Phys. Chem. C* **2008**, *112* (32), 12168–12176.

(11) Levi-Kalisman, Y.; Jadzinsky, P. D.; Kalisman, N.; Tsunoyama, H.; Tsukuda, T.; Bushnell, D. A.; Kornberg, R. D. *J. Am. Chem. Soc.* **2011**, *133* (9), 2976–2982.

(12) Jadzinsky, P. D.; Calero, G.; Ackerson, C. J.; Bushnell, D. A.; Kornberg, R. D. *Science* **2007**, *318*, 430–433.

(13) Gao, Y. *J. Phys. Chem. C* **2013**, *117* (17), 8983–8988.

(14) Manzoni, C.; Polli, D.; Cerullo, G. *Rev. Sci. Instrum.* **2006**, *77* (2), 023103.

(15) Polli, D.; Lüer, L.; Cerullo, G. *Rev. Sci. Instrum.* **2007**, *78* (10), 103108.

(16) Stoll, T.; Maioli, P.; Crut, A.; Burgin, J.; Langot, P.; Pellarin, M.; Sánchez-Iglesias, A.; Rodríguez-González, B.; Liz-Marzán, L. M.; Del Fatti, N.; Vallée, F. *J. Phys. Chem. C* **2015**, *119* (3), 1591–1599.

(17) Perdew, J. J.; Burke, K.; Ernzerhof, M. *Phys. Rev. Lett.* **1996**, *77* (3), 3865–3868.

(18) Frisch, M. J.; Trucks, G. W.; Schlegel, H. B.; Scuseria, G. E.; Robb, M. A.; Cheeseman, J. R.; Scalmani, G.; Barone, V.; Petersson, G. A.; Nakatsuji, H.; Li, X.; Caricato, M.; Marenich, A.; Bloino, J.; Janesko, B. G.; Gomperts, R.; Mennucci, B.; Hratchian, H. P.; Ortiz, J. V.; Izmaylov, A. F.; Sonnenberg, J. L.; Williams-Young, D.; Ding, F.; Lipparini, F.; Egidi, F.; Goings, J.; Peng, B.; Petrone, A.; Henderson, T.; Ranasinghe, D.; Zakrzewski, V. G.; Gao, J.; Rega, N.; Zheng, G.; Liang, W.; Hada, M.; Ehara, M.; Toyota, K.; Fukuda, R.; Hasegawa, J.; Ishida, M.; Nakajima, T.; Honda, Y.; Kitao, O.; Nakai, H.; Vreven, T.; Throssell, K.; Montgomery Jr., J. A.; Peralta, J. E.; Ogliaro, F.; Bearpark, M.; Heyd, J. J.; Brothers, E.; Kudin, K. N.; Staroverov, V. N.; Keith, T.; Kobayashi, R.; Normand, J.; Raghavachari, K.; Rendell, A.; Burant, J. C.; Iyengar, S. S.; Tomasi, J.; Cossi, M.; Millam, J. M.; Klene, M.; Adamo, C.; Cammi, R.; Ochterski, J. W.; Martin, R. L.; Morokuma, K.; Farkas, O.; Foresman, J. B.; Fox, D. J. *Gaussian 09, Revision A.02*; Gaussian, Inc.,: Wallingford CT, 2016.

(19) Hay, P. J.; Wadt, W. R. *J. Chem. Phys.* **1985**, *82* (1), 299–310.

(20) Petersson, G. A.; Bennett, A.; Tensfeldt, T. G.; Al-Laham, M. A.; Shirley, W. A.; Mantzaris, J. *J. Chem. Phys.* **1988**, *89* (4), 2193–2218.

(21) Petersson, G. A.; Al-Laham, M. A. *J. Chem. Phys.* **1991**, *94* (9), 6081–6090.

(22) Hehre, W. J.; Stewart, R. F.; Pople, J. A. *J. Chem. Phys.* **1969**, *51* (6), 2657–2664.

(23) Tlahuice, A.; Garzón, I. L. *Phys. Chem. Chem. Phys.* **2012**, *14* (20), 7321.

(24) Tlahuice-Flores, A.; Whetten, R. L.; Jose-Yacaman, M. *J. Phys. Chem. C* **2013**, *117*, 12191–12198.

(25) Varnholt, B.; Oulevey, P.; Luber, S.; Kumara, C.; Dass, A.; Bürgi, T. *J. Phys. Chem. C* **2014**, *118* (18), 9604–9611.

(26) Jiang, D.; Whetten, R. L.; Luo, W.; Dai, S. *J. Phys. Chem. C* **2009**, *113* (40), 17291–17295.

(27) Walter, M.; Akola, J.; Lopez-Acevedo, O.; Jadzinsky, P. D.; Calero, G.; Ackerson, C. J.; Whetten, R. L.; Grönbeck, H.; Häkkinen, H. *Proc. Natl. Acad. Sci. U.S.A.* **2008**, *105* (27), 9157–9162.

(28) Das, A.; Liu, C.; Byun, H. Y.; Nobusada, K.; Zhao, S.; Rosi, N.; Jin, R. *Angew. Chem. Int. Ed.* **2015**, *18*, 3140–3144.

(29) Chen, S.; Wang, S.; Zhong, J.; Song, Y.; Zhang, J.; Sheng, H.; Pei, Y.; Zhu, M. *Angew. Chem. Int. Ed.* **2015**, *54*, 3145–3149.

(30) Heaven, M. W.; Dass, A.; White, P. S.; Holt, K. M.; Murray, R. W. *J. Am. Chem. Soc.* **2008**, *130* (12), 3754–3755.

(31) Qian, H.; Eckenhoff, W. T.; Zhu, Y.; Pintauer, T.; Jin, R. *J. Am. Chem. Soc.* **2010**, *132*

(24), 8280–8281.

(32) Lopez-Acevedo, O.; Tsunoyama, H.; Tsukuda, T.; Häkkinen, H.; Aikens, C. M. *J. Am. Chem. Soc.* **2010**, *132* (23), 8210–8218.

(33) Pei, Y.; Lin, S.; Su, J.; Liu, C. *J. Am. Chem. Soc.* **2013**, *135* (51), 19060–19063.

(34) Xu, W. W.; Gao, Y. *J. Phys. Chem. C* **2015**, *119* (25), 14224–14229.

(35) Fernández, E. M.; Soler, J. M.; Garzón, I. L.; Balbás, L. C. *Phys. Rev. B* **2004**, *70* (16), 165403.

(36) Jalbout, A. F.; Contreras-Torres, F. F.; Perez, L. A.; Garzón, I. L. *J. Phys. Chem. A* **2008**, *112* (3), 353–357.

(37) Li, Y.; Galli, G.; Gygi, F. *ACS Nano* **2008**, *2* (9), 1896–1902.